IEEE Access
Multidisciplinary ⋮ Rapid Review ⋮ Open Access Journal

Received 13 October 2023, accepted 1 November 2023, date of publication 8 November 2023, date of current version 1 December 2023.

Digital Object Identifier 10.1109/ACCESS.2023.3331590

STANDARDS

Stretchable and Bendable Polydimethylsiloxane-Silver Composite Antenna on PDMS/Air Gap Substrate for 5G Wearable Applications

SHAKHIRUL MAT SALLEH[1,2], MOHD FADZIL AIN[1], ZULKIFLI AHMAD[3], INTAN SORFINA ZAINAL ABIDIN[1] (Member, IEEE), LEE YENG SENG[2] (Senior Member, IEEE), AND MOHAMED NASRUN OSMAN[2]

[1]School of Electrical and Electronic Engineering, Universiti Sains Malaysia, Nibong Tebal, Penang 14300, Malaysia
[2]Advanced Communication Engineering (ACE), Centre of Excellence, Faculty of Electronic Engineering and Technology, Universiti Malaysia Perlis, Arau, Perlis 02600, Malaysia
[3]School of Materials and Mineral Resources Engineering, Universiti Sains Malaysia, Nibong Tebal, Penang 14300, Malaysia

Corresponding author: Mohd Fadzil Ain (eemfadzil@usm.my)

This work was supported by the Ministry of High Education Malaysia through the Fundamental Research Grant Scheme under Grant FRGS/1/2023/TK07/USM/01/1.

ABSTRACT An engineered composite conductor is essential for developing a wearable antenna that is not only flexible but also stretchable. This paper presents the use of polydimethylsiloxane (PDMS) as the substrate and custom polydimethylsiloxane-silver conductive paste for wearable applications. The antenna is designed with an air gap PDMS substrate between the patch and sawtooth partial ground at 3.5 GHz to enhance the bandwidth and gain. Furthermore, the proposed antenna is flexible and can be bent as well as stretched up to 20%, making it suitable for use on the human body. This study investigates the antenna's performance under bending and stretching to mimic the human body's structure and movements. Additionally, the specific absorption rate (SAR) of the wearable antenna was analyzed for safety purposes.

INDEX TERMS Wearable antenna, stretchable, bendable, silver conductive paste, 5G applications.

I. INTRODUCTION

Fifth generation (5G) wireless communications are expected to overcome current wireless network issues by providing new frequency bandwidth, high data rates, low latency, a manifold increase in base station capacity, and a significant improvement in the user's perceived quality of service (QoS). In conjunction with conventional microwave frequencies, the 5G architecture offers a highly dense, diversified, and versatile technology with extra bandwidth availability for almost unlimited upgradation [1]. Thus, exploring new less-congested spectrum bands, such as the 3.5 GHz band under the middle band of 5G frequencies [2], is a great solution to increase network capacity. One of the biggest trends in current and upcoming 5G networks is the integration of devices with the world of wearable technology applications.

The associate editor coordinating the review of this manuscript and approving it for publication was Pavlos I. Lazaridis.

Wearable devices are those that can be worn by a person and have the capability to connect with each other directly or through their embedded wireless modules, which interoperate with other components such as batteries, sensors, and/or antennas [3], [4], [5].

Wearable technology is anticipated to play a crucial role in 5G technology and Internet of Things (IoT) ecosystems [6]. According to Cisco's Virtual Networking Index (VNI) annual report (2014-2019) [7], the amount of data traffic generated by wearable devices is projected to increase to 277 petabytes per month by 2019, and the number of such devices is expected to reach 578 million by the same year. This represents a five-fold increase from that in 2014. Wearable devices are defined as personal wearable items that can connect to each other or through embedded cellular connectivity. They communicate with external devices via built-in wireless modules, which comprise components such as batteries, sensors, and antennas.

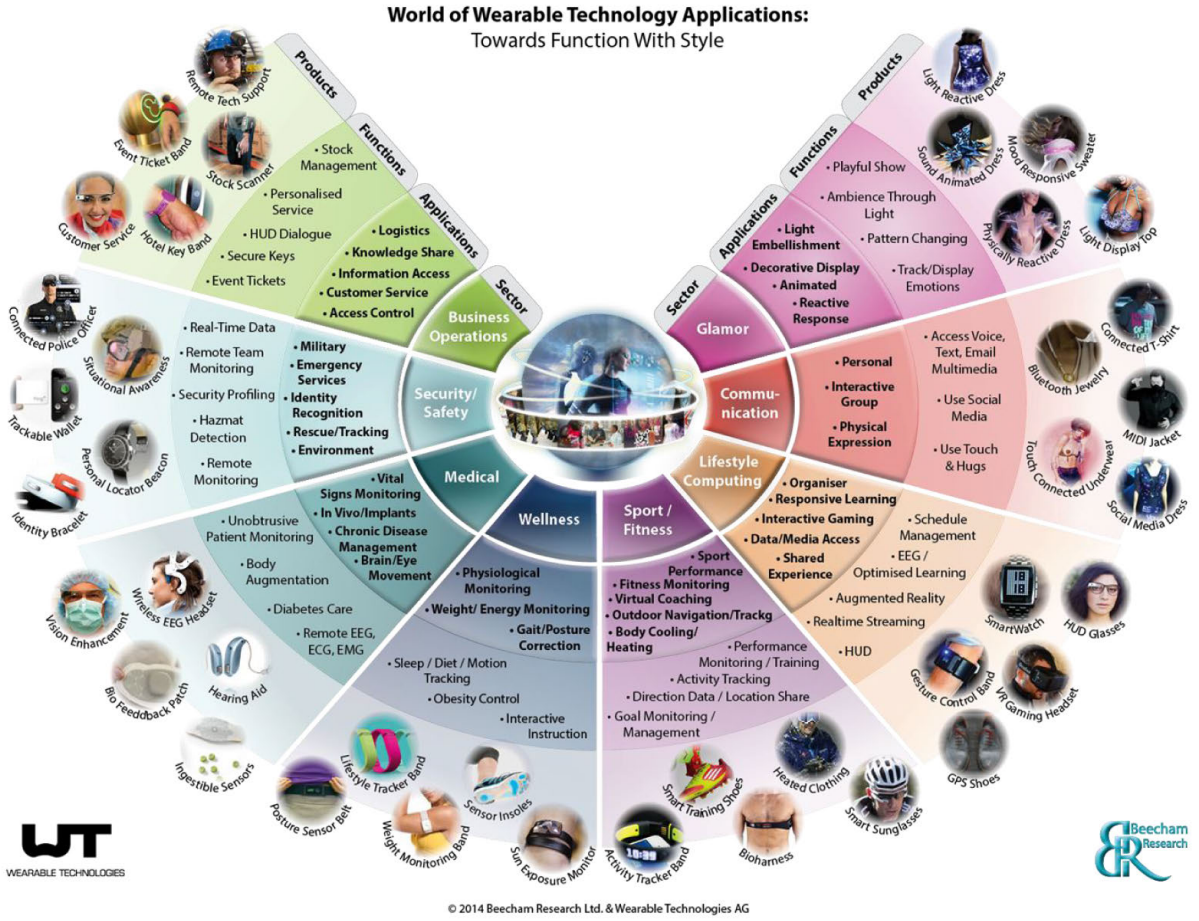

FIGURE 1. World of wearable technology [4], [9].

A visual representation of the various technologies that will be utilized in wearable 5G networks is shown in Figure 1, which shows that wearable technology has a broad range of applications in daily life. It extends beyond wristwatches, fitness bands, and encompasses numerous medical applications [8]. In healthcare augmented reality glasses, and wearable devices are utilized to monitor critical health parameters of patients, such as glucose monitoring systems, capsule endoscopy to examine the gastrointestinal system, wearable doppler units, and thermometers to monitor the heart rate, blood pressure, and body temperature. Additionally, wearables have applications in entertainment and rescue operations, such as augmented reality glasses and smartwatches that serve as touch screen computers. Wearable technology can also be integrated into clothing, footwear, protective gear, and rescue equipment in emergency response systems.

In contrast to conventional rigid antennas, wearable antennas are primarily attached to the human body for wireless body sensor networks, which require particular considerations such as light weight, flexibility, robustness, ease of interpretation, and user comfort. Thus, while developing wearable antennas, the choice of material used is crucial. Previous researchers preferred to use fabric materials, such as cotton, wool, felt, fleece, and denim/jeans as substrates. Meanwhile conductive thread, Shieldit Supper, Flectron, and copper sheet/tape were used as patch and ground, since they offer flexibility. However, it is worth noting that they are not stretchable [10], [11], [12], [13]. Hence, using polydimethylsiloxane (PDMS) as the substrate for wearable antennas has become a popular choice because of its low Young's modulus ($<$3 MPa), implying high flexibility and stretchability, which allows for more freedom and control of user motion [14]. Moreover, PDMS also offers thermal stability, homogeneity, relative isotropic, an acceptable loss in the microwave region with low permittivity and high volume resistivity, which helps prevent the generation of parasitic currents in the substrate [15]. However, previous studies used PDMS substrates embedded with conductive fabric [16], [17], [18] and PDMS-copper foil [19], [20], [21], [22], which are rigid conductive materials that limit the stretchability of the antenna package.

Thus, in this study, a custom-made flexible silver-PDMS (Ag-PDMS) composite conductive paste based on a PDMS

substrate is proposed for wearable antenna applications. The typical microstrip patch antenna is designed on a microwave laminate/ printed circuit board or even a textile antenna, where the conductive patch and substrate thickness are dependent on the manufacturers' specifications which are not controlled by the designers. Therefore, using a custom-made material gives designers the flexibility to vary the conductivity patch value and the thickness of the substrate to achieve the desired characteristics of a wearable antenna. To achieve the specifications of a wearable antenna, the conductive paste formulated to strongly adhere to the PDMS substrate antenna was analyzed, so it's does not crack when subjected to mechanical deformation, such as bending and stretching.

As with any wearable antenna, the antenna structure is affected by the need to conform to the human body shape and body movements thereby affecting the antenna's performance. There a lack of study in the area of antenna bending and stretching analysis in a single microstrip patch antenna. Most of the textile antennas focused on bending analysis [23], [24], [25], [26], whereas other researchers have only focused on stretching analysis [20], [27], [28]. Thus, this study investigated the effects of bending and stretching wearable antennas to enhance our understanding of their performance under such deformations. Furthermore, this study also conducted a Specific Absorption Rate (SAR) analysis to ensure the safety of the proposed wearable antenna for use on the human body.

II. METHDOLOGY

This section discusses the methodology concerning the design and development of a polydimethylsiloxane-silver composite wearable antenna.

A. SUBSTRATE PPREPARATION

PDMS, commercially available as Sylgard 184, comes in liquid form in two parts: a base and a curing agent. The PDMS substrate sample was prepared by mixing the base and curing agents at a ratio of 10:1. The amount of base and curing agent required was measured using a digital scale in grams based on the mould size. The acrylic mould size of 40 × 40 × 2 mm^3 was custom-made and prepared earlier. Next, the sprayer remover mould was applied into a rectangular acrylic mould before the PDMS mixture was poured, so that the cured PDMS could be easily removed from the mould. After that, the PDMS substrate was treated under vacuum suction to remove air bubbles and then cured under thermal curing at 100 °C for over 35 minutes, as shown in Figure 2.

A major constraint in the design of microstrip patch antennas is that the dielectric properties of the materials used reflect the size and antenna operating frequency. Unlike, the well-known rigid commercial boards (RF4, Rogers, or Taconic), the dielectric properties are available even in the Computer Simulation Technology (CST) software library. However, for custom-made substrates such as PDMS, it is important to measure the dielectric properties and create a 'new material' with a specific dielectric value of PDMS while designing the antenna using CST software. Even though PDMS dielectric properties are available, the value can vary between different suppliers or even different batches of the same supplier. In addition, the dielectric properties are generally not constant in frequency and are dependent on the mixture, orientation, and molecular structure of the material [29]. Hence, it is suggested to have your own dielectric properties measurements for selected materials at a particular operating frequency before start to designing antenna rather than cite other paper.

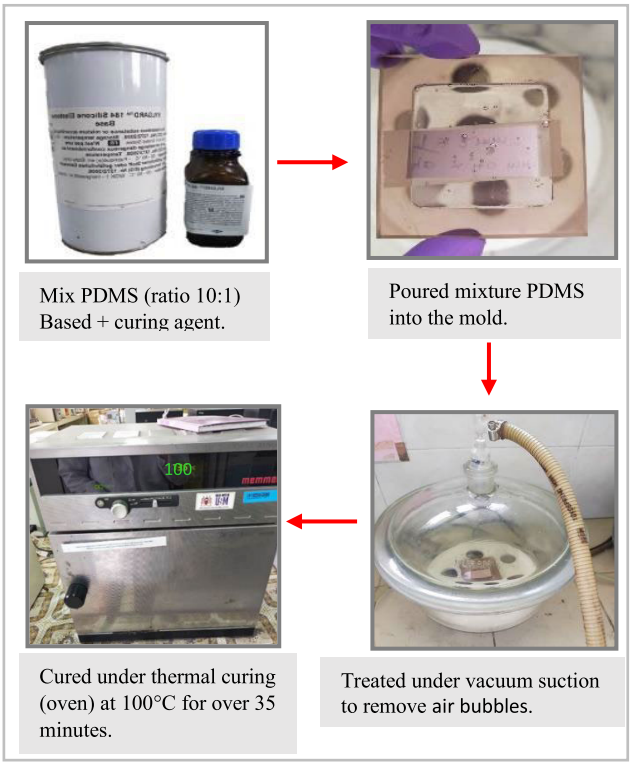

FIGURE 2. Overall process of PDMS substrate fabrication.

In this study, an open-ended coaxial probe method was used to measure the dielectric properties of the PDMS substrate. The measurement system consisted of an Agilent 85070D High Temperature Dielectric Probe Kit, Agilent E5071C P-Series Network Analyzer (PNA), Agilent material characterization software, and a laptop (optional) used as an extension window. This probe is suitable for measuring solid or semi-solid materials, as well as liquids, over broadband frequency ranges. For this type of measurement, good contact between the Material Under Test (MUT) and probe is very important. Another criterion is that the MUT has a smooth flat surface, and the diameter of the sample (>20 mm) is much larger than the open-ended coaxial probe aperture. Any insufficient contact or a rough surface reduces the measurement accuracy by several orders of magnitude.

Figure 3 shows that, the measured dielectric constant, ε_r' and dielectric loss factor, ε_r'' at 3.5 GHz are 2.74 and 0.157, respectively. Meanwhile, the dissipation factor of the

material, also known as the electrical loss tangent, tan δ is 0.057. It can be obtained using equation (1) [30].

$$\tan\delta = \varepsilon''/\varepsilon' \tag{1}$$

The measured dielectric constant of PDMS substrate is in good compliance with other works, where ($\varepsilon'_r = 2.65$, tan $\delta = 0.02$ at 2.42 to 2.52 GHz) [31], ($\varepsilon'_r = 2.8$, tan $\delta = 0.02$ at 2.45 GHz) [32], ($\varepsilon'_r = 2.76$, tan $\delta = 0.03$ at 0.2 to 5 GHz) [33], ($\varepsilon'_r = 2.7$, tan $\delta = 0.019$ at 2.4 GHz) [20], ($\varepsilon'_r = 2.68$, tan $\delta = 0.02$ at 2.45 GHz) [34], and ($\varepsilon'_r = 2.5$ - 3.0, tan $\delta = 0.01$ - 0.05 at 0.5 to 3 GHz) [35]. On the other hand, the dielectric constant, ε'_r of the PDMS used was 2.74 were, which is range ($2.2 \leq \varepsilon'_r \leq 12$) for typical dielectric constant substrates for microstrip antennas [36].

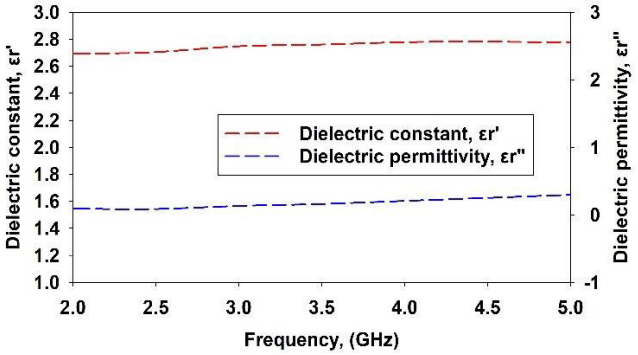

FIGURE 3. Measured dielectric properties of PDMS substrate.

B. PREPARATION OF CONDUCTIVE Ag-PDMS PASTE COMPOSITE

The preparation of conductive materials composite consists of silver (Ag) powder in the size range of 2-3.5 μm. The poly(dimethylsiloxane) hydroxyl (OH-PDMS) terminated with an average molecular weight (M_n) of 110×10^3 g/mol and a viscosity of 50×50 cSt functioned as an intermediate between silver and the PDMS substrate. Cyclotetrasiloxane (D4), containing four repeating units of silicone (Si) and oxygen (O) atoms in the closed loop cycle used to make OH-PDMS, became more liquid. Therefore, it could be easily mixed with the silver powder. (3-glycidyloxypropyl)-trimethoxysilane (ETMS) and (3-trimethyloxysily) propyl methacrylate (ATMS) were used as additives to improve the processability and productivity of Ag-PDMS composites by enhancing adhesion. Vinyltrimethoxysilane (VTMS) was used as the coupling agent, and dibutyltin dilaurate (DBTDL) was used as the curing agent [37], [38], [39].

The Ag-PDMS conductive paste sample was fabricated using 65 wt% silver powder; OH-PDMS (0.2g), D4 (250 μL), ETMS, VTMS, and ATMS (10 μL each) were mixed by magnetic stirring for 10 minutes at 210 rpm. The curing agent DBTDL (5 μL) was added to the mixture and stirred momentarily before a squeegee was printed onto the PDMS substrate, as previously described in Section A. To create a conductive strip that can strongly adhere to the stretchable PDMS substrate, the entire package was then thermally cured for 40 minutes at 60°C. Unlike the approach provided in [37], this study did not employ ultrasonication, that might break the polymer chain and release heat, which will continually speed up the curing process. As a result, the working window time was shortened, particularly during the squeegee printing process. Figure 4 illustrates the overall process of Ag-PDMS conductive paste fabrication on the PDMS substrate sample.

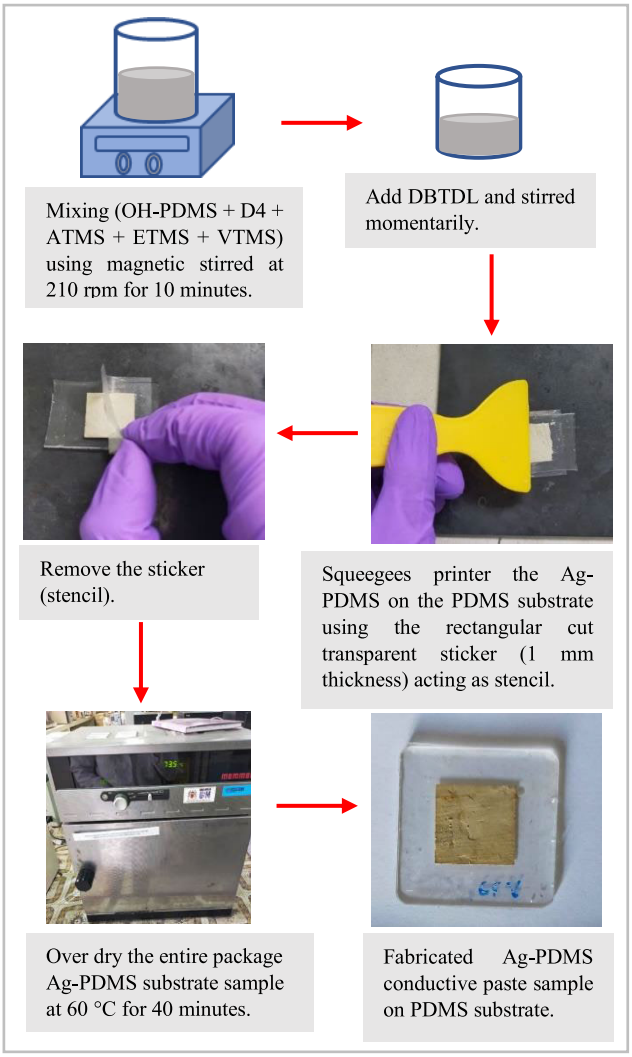

FIGURE 4. Overall process of Ag-PDMS conductive paste sample fabrication.

Usually, the conductivity parameters of copper cladding on well-known rigid boards such as FR, Rogers, or Taconic which are used for fabricating conventional antennas are available from suppliers or even in the CST software library. However, unlike the custom-made Ag-PDMS composite paste used in this study, its conductivity needs to be measured. Thus, the four-point collinear probe measurement method was used to measure the Ag-PDMS conductivity in this study, using the Keithley 4200A-SCS parameter analyzer from Tektronix and the MPI TS50 manual probe system.

The conductivity of Ag-PDMS conductive paste was measured four times, and the resulting average was 6.58×10^6 S/m.

C. ANTENNA DESIGN

Firstly, a rectangular patch antenna was designed and simulated at 3.5 GHz. A rectangular patch antenna named Antenna Step 1, made of a PDMS substrate with a thickness of 2 mm and fully ground at the back with a conductive thickness of 0.1 mm. The overall dimension of Antenna Step 1 is shown in Figure 7. The conventional geometry of a rectangular patch antenna has certain limitations. It is inherently narrowband and exhibits less ideal matching due to its resonant characteristics. This is because the patch dimensions are finite along the length and width, leading to fringing of fields at the edges of the patch. The extent of fringing depends on the patch dimensions and the substrate height [36]. When electromagnetic waves are radiated or received by the rectangular patch antenna, they interact with the edges of the finite-sized patch. This interaction causes the electric and magnetic fields to extend or ''fringe'' beyond the physical boundaries of the patch. The extent of this fringing effect is influenced by the dimensions of the patch (length and width) and the height of the substrate on which the patch is mounted. The fringing of fields at the edges can affect the behaviour of the antenna, such as its radiation pattern, impedance matching, and bandwidth.

To address this issue, one approach is to design the antenna with thicker substrates having a lower dielectric constant. This choice offers several advantages, including improved efficiency, a wider bandwidth, and loosely bound fields for efficient radiation into space. However, a trade-off exists as thicker substrates with lower dielectric constants result in larger element sizes [40]. On the other hand, for microwave circuitry applications, thin substrates with higher dielectric constants are preferred. These substrates require tightly bound fields to minimize unwanted radiation and coupling, leading to smaller element sizes and better integration in compact circuits [40].

Hence, for this research, the initial design of a rectangular patch antenna starts with the parameter study of PDMS substrate thickness. The parameter study is to evaluate the PDMS thickness at (1, 1.2, 1.4, 1.6, 1.8, and 2.0) mm. This value is calculated by considering the fabrication process and PDMS flexibility. The fabrication of PDMS with a thickness of less than 1 mm is challenging (to make thin mould) as the substrate could break easily when stretched. Meanwhile, a substrate thickness of more than 2 mm will make PDMS stiffer and less flexible.

Figure 5 shows the simulated reflection coefficient, S_{11} of patch antenna Step 1 at different substrate thickness. The result indicates that the increase in substrate thicknesses will increase antenna bandwidth and improve the impedance matching of S_{11}. Moreover, the gain of patch antennas increases with the increase in substrate thickness, as shown in Figure 6. It can be observed that, when the substrate thickness increases, a volume of fringing effect occurs between the edge of the patch and the ground plane, (which is a substrate between the patch and ground) leading to better antenna performance [41]. Since the fringing effect is reflected in the effective dielectric constant, the parameters involved are the width of the patch, the dielectric constant of substrate and thickness of the substrate (by referring to equation 3). In this set of observations, the best substrate thickness for this proposed antenna Step 1 was 2 mm. The optimization of patch length was conducted at every changing of substrate thickness to get a centre frequency of 3.5 GHz. The patch length is decreased by about 0.6 to 0.8% at every 0.2 mm increases in PDMS thickness. This is due to the inherent nature of microstrip antennas, as can be observed through the utilization of equations (2), (3), and (4) [36]. Equation (2) represents a method for determining the optimal width of the patch, denoted as ''W'', which yields favorable radiation efficiencies. This width is ascertained using the formula:

$$W = \frac{c}{2f_r}\sqrt{\frac{2}{\varepsilon_r + 1}} \tag{2}$$

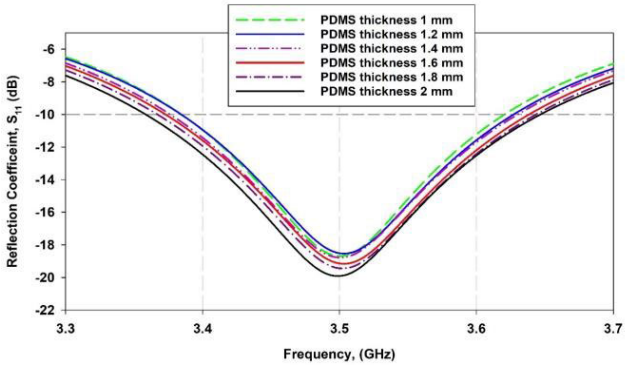

FIGURE 5. Reflection coefficient, S_{11} of substrate thickness analysis.

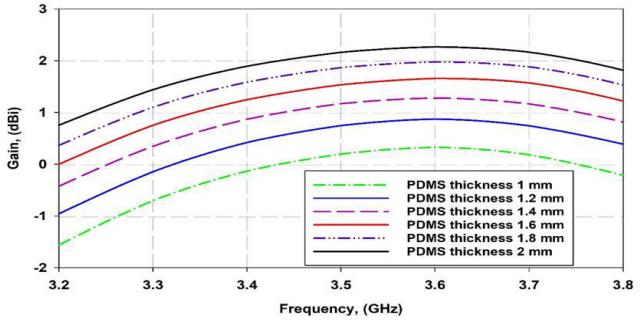

FIGURE 6. Gain of substrate thickness analysis.

Here, C signifies the velocity of free space, fr denotes the resonant frequency, and εr represents the dielectric constant of the substrate material.

Moreover, equation (3) provides insight into the patch length at the resonant frequency. This length, denoted as ''L'',

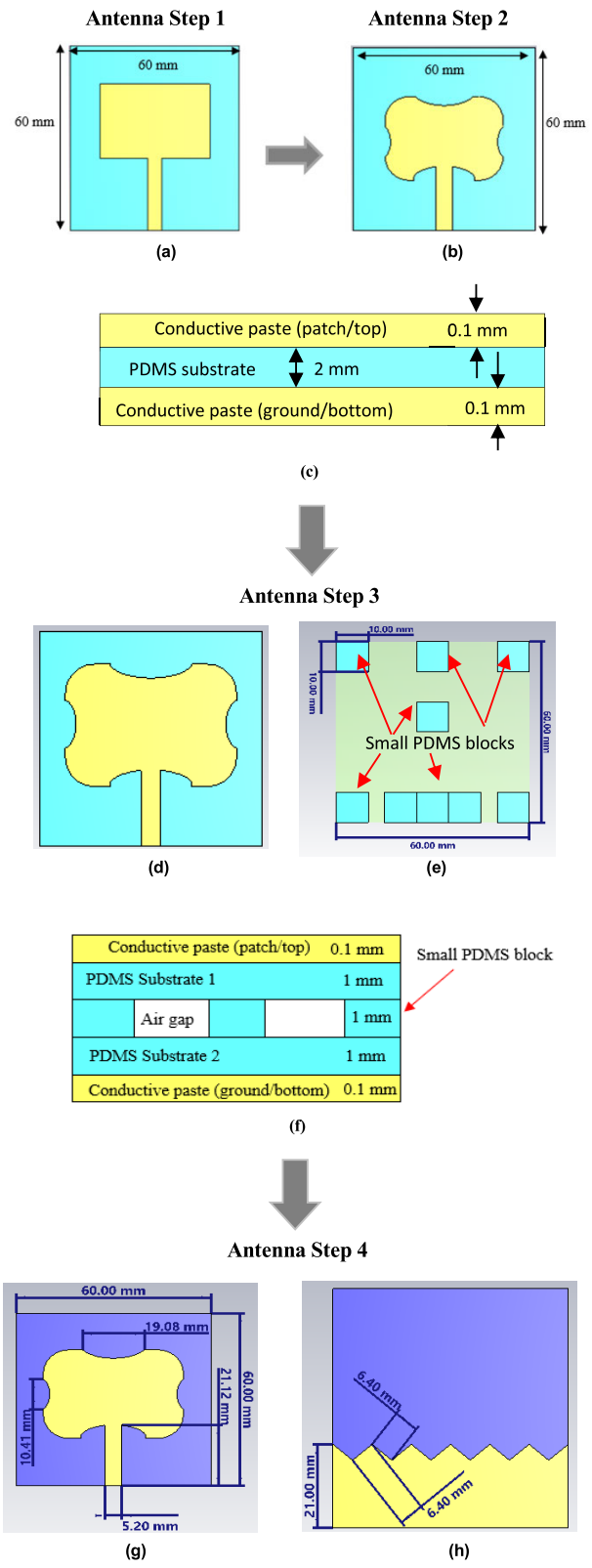

FIGURE 7. Overall step of antenna proposed design (a) Front view antenna Step 1 (b) Front view antenna Step 2 (c) Rear view antenna Step 1 and 2 (d) Front view of substrate 1 (e) Front view of substrate 2 (f) Rear view antenna Step 3 (g) Front view of substrate 1 (h) Front view of substrate 2.

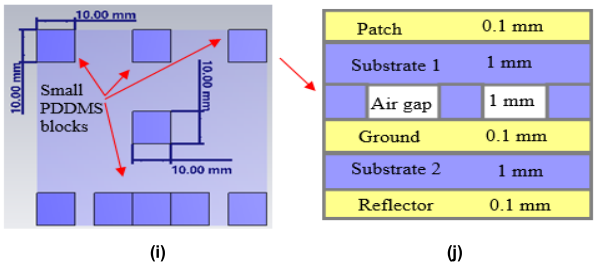

FIGURE 7. *(Continued.)* Overall step of antenna proposed design (i) Small PDMS blocks between substrate 1 and 2 (j) Rear view antenna Step 4.

is determined while accounting for the fringing field effect and is given by:

$$L = \frac{c}{2f_r\sqrt{\varepsilon_{eff}}} - 2\Delta L \tag{3}$$

In equation (3), ε_{eff} corresponds to the effective dielectric constant of the substrate material, which can be expressed as per equation (4):

$$\varepsilon_{eff} = \frac{\varepsilon_r + 1}{2} + \frac{\varepsilon_r - 1}{2}\left(\frac{1}{\sqrt{1 + 12\frac{h}{W}}}\right) \tag{4}$$

where, h signifies the thickness of the substrate. Additionally, an additional parameter ΔL is introduced due to the fringing field effects at the radiating edge, and its value is calculated according to equation (5):

$$\Delta L = h0.412\frac{(\varepsilon_{reff} + 0.3)\left(\frac{W}{h} + 0.264\right)}{(\varepsilon_{reff} - 0.258)\left(\frac{W}{h} + 0.8\right)} \tag{5}$$

With these equations in consideration, the substrate thickness, h is nonlinear to the patch length, L. In other words, the increase in substrate thickness will affect the effective dielectric constant, ε_{eff}, which leads to a decrease in patch antenna length. Additionally, for patch antennas, the length, L of the element is usually $\lambda_0/3 \leq L \leq \lambda_0/2$ [36], and the substrate thickness analysis (1 to 2 mm) resulted in the patch length optimization being in the range as suggested.

Subsequently, in pursuit of enhanced antenna performance, the design of Antenna Step 2 involves the integration of slits along the right, left, upper, and lower edges of the rectangular patch utilized in Antenna Step 1. Prior researchers have successfully elevated impedance matching, bandwidth, and gain through the application of slit antenna techniques [42], [43], [44], [45]. The strategic implementation of slits on the patch radiator contributes to an improved impedance match, particularly at higher frequencies. These introduced slits induce modifications in the current distribution across the radiator, consequently influencing current path lengths and impedance at the input point [46]. Moreover, the incorporation of slits, achieved by eliminating segments from the four edges of the original rectangular patch, indirectly reduces the overall patch dimensions and subsequently lowers production costs.

Although applying the slits at the patch can improve the reflection coefficient, S_{11} of antenna Step 1, the antenna's performance is still not satisfactory. Thus, for antenna Step 3, an air gap was introduced between substrate 1 (1 mm thickness) and substrate 2 (1 mm thickness) as shown in Figure 7 (e) and (f). The top of substrate 1 contained a patch antenna, and a fully ground antenna at the bottom of substrate 2. Finally, to enhances the antenna's performance, step 4 was proposed. In antenna Step 4, the sawtooth partial ground, and reflector were integrated while maintaining the patch shape and air gap from Step 3. The first layer of the substrate (1 mm thick) contained an antenna patch at the front. The second substrate (1 mm thick) had a sawtooth partial ground at the top and was fully conductive at the back, acting as a reflector. Small PDMS blocks were steak/glue between substrates one and two to create an air gap of 1 mm thickness. The size and placement of the PDMS block were finalised by considering the overall size of the substrate. Nine PDMS blocks, each measuring 10 × 10 mm, were extensively tested extensively to provide adequate support for the first and second substrates, creating an air gap between them. The PDMS blocks were strategically positioned at the edges and middle of the substrates to ensure a sturdy structure. Additionally, extra PDMS blocks were placed at the bottom of the substrate to support the placement of the SMA connector. Meanwhile, the 1 mm thickness of PDMS substrate for each layer was chosen for antenna 4 instead of 2 mm, which is to minimize the antenna size and at the same time, provide more flexibility during the stretching. Moreover, the fabrication of PDMS substrates with thicknesses below 1 mm is more challenging, and the substrate can easily break during stretching. Meanwhile, the fabrication of a PDMS substrate with a thickness of more than 2 mm increases the stiffness and reduces the flexibility of bending and stretching. Figure 7 shows the overall steps of the proposed antenna design evolution.

1) REFLECTION COEFFICIENT AND GAIN ANTENNA COMPARISON

The simulated reflection coefficient, S_{11} for the four-step antenna design evolution is shown in Figure 8. Antenna Step 1 produces the reflection coefficient, bandwidth and gain of −19.89 dB, 285 MHz and 2.16 dBi respectively at 3.5 GHz. In Step 2, the reflection coefficient was improved up to −30.19 dB but the bandwidth and gain slightly decreased to 234 MHz and 2.14 dBi respectively. As illustrated in Figures 8 and 9, the presence of an air gap in Step 3 can enhance the reflection coefficient and gain up to −40.54 dB and 5.80 dBi respectively. Air has a low permittivity and is used as a substrate, consequently changing the volume of the fringing effects, leading to an effective gain and reflection coefficient [47].

Next, the integrated sawtooth partial ground and reflector in Step 4 can enhance the reflection coefficient, S_{11} and gain of -58.63 dB and 6.23 dBi respectively. The increase in operative S_{11}, when the sawtooth partial ground plane was introduced is due to the distributed modulation of the distance between the ground plane and the lower part of the patch. Such modulation allows for a more effective electromagnetic coupling between the ground plane and the patch, resulting in better S_{11} [48], [49]. Meanwhile, the integrated reflector at the back, helps redirect the radiated energy from back the to the front. This can increase the power density in the front lobe antenna, which can lead to a higher gain. The presence of a reflector in the microstrip patch increases the gain of the antenna, which is consistent with the results of other studies [50], [51], [52]. Although, the bandwidth in Step 4 was slightly decreased to 234 MHz, it already met the targeted results for the operating bandwidth for 5G applications. Therefore, the antenna designed in Step 4 was chosen for fabrication and the prototype antenna was tested for validation.

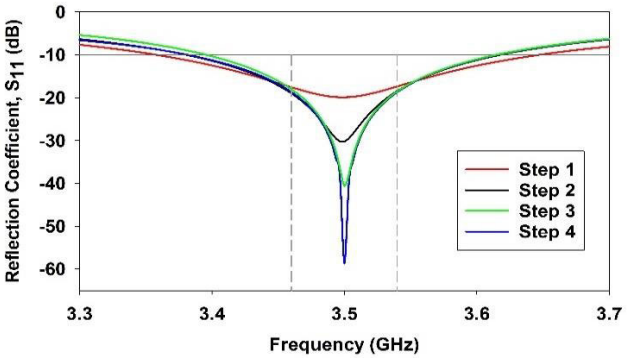

FIGURE 8. Simulated reflection coefficient, S_{11} of antenna Step 1, 2, 3, and 4.

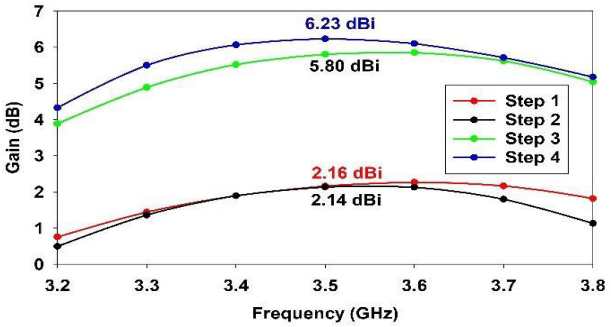

FIGURE 9. Simulated antenna gain Step 1, 2, 3, and 4.

2) ANTENNA DIRECTVITY COMPARISON

Figure 10 shows the directivity of antenna steps 1, 2, 3, and 4 across the frequency range of 3.2 to 3.9 GHz. Antenna Step 1 has an average directivity of 7.46 dBi and maximum directivity of 7.54 dBi at 3.7 GHz. For antenna Step 2, the average directivity was 7.77 dBi and the maximum directivity was 7.92 dBi at 3.7 GHz. Meanwhile, for antenna Step 3, the average directivity was 8.45 dBi and the maximum directivity

was 8.66 dBi at 3.7 GHz. Meanwhile, the average directivity and maximum directivity at 3.6 GHz for antenna Step 4 were 8.61 and 8.71 dBi, respectively. The increases in the directivity of the antenna from Step 1 to Step 4 was aligned with the increased performance of the antenna reflection coefficient and gain [36].

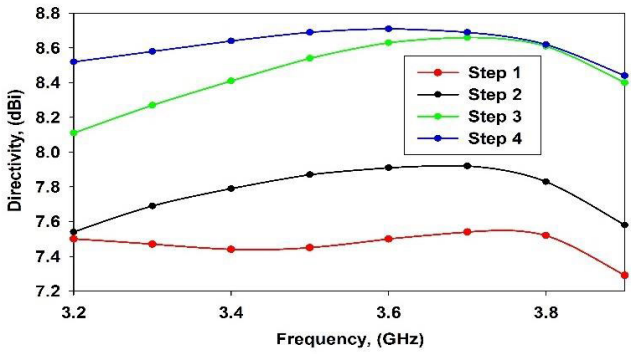

FIGURE 10. Simulated directivity of antenna Step 1, 2, 3, and 4.

3) RADIATION PATTERN COMPARISON OF ANTENNA STEP 1, 2, 3, AND 4

The comparison radiation patterns of antenna steps 1, 2, 3, and 4 are plotted in the X-Z plane as shown in Figure 11. It was observed that all the antenna steps operated in the forward directional with a minor lobe at the back, which is beneficial for wearable antenna applications. The major lobe radiation pattern significantly increases from antenna Step 1 to antenna Step 4. Meanwhile, the improved technique applied in designing antenna Step 2 up to antenna Step 4 substantially reduced the back-lobe radiation. The reduction of back-lobe radiation in wearable antenna applications significantly reduces the specific absorption rate (SAR)/ electromagnetic radiation towards the human body.

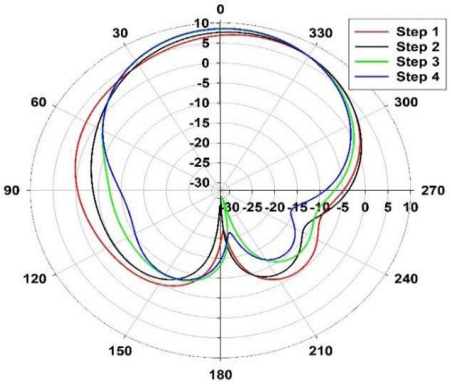

FIGURE 11. Simulated radiation pattern in X-Z plane of antenna Step 1, 2, 3, and 4.

4) SURFACE CURRENT COMPARISON

In general, a uniform distribution of current on the surface of the patch antenna is desired, as it results in a more efficient current flow, a better radiation pattern, and a higher gain [36]. The patch's radiation is usually treated as radiation from two magnetic dipoles located at each end of the patch. These magnetic dipoles travel along the length of the slots and are in phase with each other. However, not much radiates on the sides of the patch compared to the gaps at the edges of the patch. Most electrical currents are directly beneath them on the underside of the patch and the ground plane, as they are on the microstrip. The patch and ground currents are close together and hidden in opposite directions by the patch, which is why these currents do not radiate, as shown in Figure 12 (blue region on the patch). Figure 12 depicts the surface current distribution plot at 3.5 GHz for antenna steps 1, 2, 3, and 4 based on the simulation. The results show that the application of slits in Antenna Step 2 leads to a more uniform surface current distribution on the edges of the patch antenna compared to Antenna Step 1, which exhibits green and yellow areas on the edges. Furthermore, Antenna Step 3 demonstrates improved suppression (more blue colour) at the edges of the patch owing to the inclusion of an integration air gap between the patch and ground. Finally, the implementation of a sawtooth partial ground and reflector in Antenna Step 4 effectively filters the undesired surface current by achieving a matching impedance between the upper sawtooth partial ground and the lower part of the patch. Antenna Step 4 exhibits a larger suppression area around the edges of the patch compared to the other Antenna Steps, indicating a more uniformly distributed current.

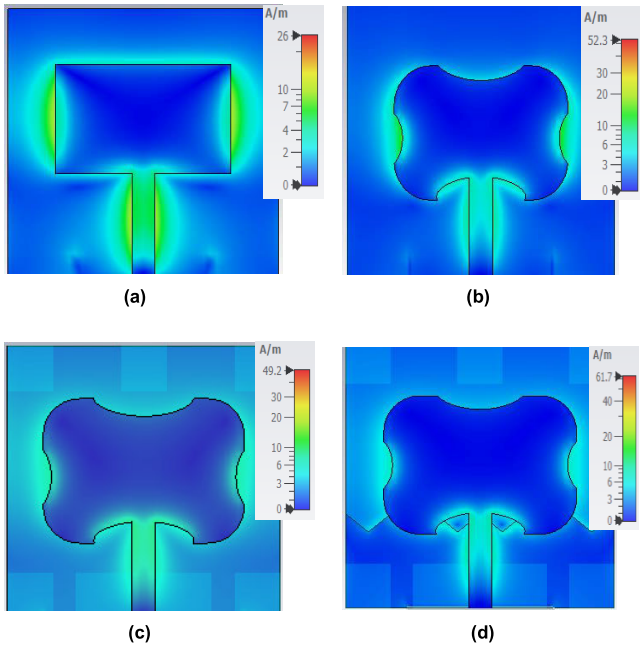

FIGURE 12. Simulated surface currents of antenna (a) Step 1, (b) Step 2, (c) Step 3, and (d) Step 4.

D. ANTENNA FABRICATION

After evaluating the simulated performance, the antenna design in Step 4 was deemed the most optimal and was thus

selected as the final design. The antenna was subsequently fabricated to facilitate experimental verification. Because the fabrication process for the proposed antenna is completed in-house and requires manual customization, additional precautions are necessary due to the use of potentially hazardous chemicals. Initially, the PDMS substrate was fabricated using a method similar to the PDMS preparation sample outlined in Section II-A, with the exception of using a mould size larger than the sample mould size. Consequently, more time was required to extract air bubbles from the PDMS substrate.

Additionally, the fabrication process for the silver (Ag) conductive paste is applied using a process similar to that detailed in Section II-B, which outlines the fabrication of conductive material samples. During this process, a cutting printer (Silhouette Cameo 3) was used to cut transparent stickers with a thickness of 0.1 mm, which functioned as stencils. The proposed antenna design is exported from CST accordingly, and the patch antenna dimensions are transferred to Silhouette Studio printer software for the cutting process. The cut patch antenna dimension stickers are then placed on the PDMS substrate to squeegee print the silver paste, with the stencil sticker removed once the squeegee has been printed and is ready for curing. The same technique was applied to the squeegee print of conductive paste on the ground plane antenna.

An SMA connector, also known as a SubMiniature version A connector, was employed to connect the patch antenna to the edge feed line. The silver conductive epoxy adhesive 8330S, sourced from M.G. Chemicals in Canada, was utilized as an adhesive between the SMA and the antenna. This adhesive comprises two components, silver, and adhesive, which are mixed in equal proportions as depicted. Subsequently, the entire antenna assembly was thermally cured at 65°C for two hours to enhance the SMA's adhesion to the stretchable antenna. Figure 13 shows the manufactured prototype antennas.

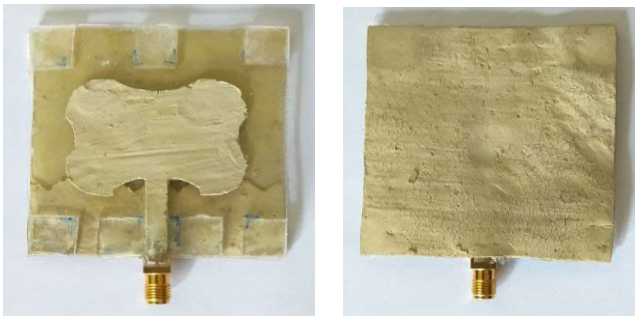

(a) (b)

FIGURE 13. Fabricated antenna prototype Step 4 (a) front view and (b) back view.

Surface roughness in patch antenna design can have a significant impact on antenna performance. Research studies [53], [54], [55] have shown that surface roughness affects the conductivity of both the patch and the ground used in antenna construction, leading to potential degradation in overall performance. Specifically, surface roughness can considerably reduce the antenna's efficiency and gain [54], adversely affecting its ability to radiate and receive electromagnetic waves effectively. Studies conducted at millimeter-wave frequencies [55] have revealed that surface roughness has a particularly noteworthy effect on antenna arrays, resulting in increased antenna losses and reduced efficiency and gain. The degradation caused by surface roughness can have a more substantial impact on high-frequency antennas compared to those operating in the lower or middle bands. One key reason for this difference lies in the relative size of the antenna components with respect to the wavelength at different frequency ranges. At lower or middle frequencies, the wavelengths are longer, and the physical size of the patch antenna becomes relatively larger as well. Consequently, the impact of surface roughness on the patch's surface becomes less significant in terms of wavelength fractions. Conversely, at higher frequencies, the wavelengths are shorter, and the physical size of the patch antenna is relatively smaller, making it more sensitive to even minor irregularities on the surface. It is important to highlight that the proposed antenna in this research is designed to operate in the middle frequency range, thus, the surface roughness at the patch and ground will have less impact on antenna performance compared to the millimeter wave antenna.

III. RESULT AND DISCUSSION

This section discusses the analysis of the performance of the Step 4 prototype antenna concerning the reflection coefficient, S_{11}, gain, directivity, and radiation pattern under normal (flat), stretching, and bending conditions.

A. SIMULATED AND MEASURED ANTENNA

The simulated and measured reflection coefficient, S_{11} of the antenna in Step 4 is shown in Figure 14. The measured antenna prototype was shifted to high frequencies (3.54 GHz) with a slightly decreased bandwidth of 220 MHz compared to the simulated 234 MHz. The shifted frequency of the prototype antenna was due to the manual process employed, some thickness variation of PDMS was inevitable, and the use of glue to combine substrates 1 and 2 was not considered in earlier simulations. However, the S_{11} of the prototype antenna is in good agreement with the targeted bandwidth of 5G applications.

To verify the discrepancies between the simulated and measured results, antenna Step 4 was redesigned and simulated by considering the existence of thin glue layers between the substrates. The electrical properties of the UHU glue used in antenna Step 4 were measured using a performance probe (Keysight 85070E), resulting in dielectric constants and loss tangents of 8.44 and 0.11, respectively at 3.5 GHz. Since the thickness of the glue is uncertain and the value cannot be determined accurately, hence, the analysis of the thickness of the glue; (*Tg1* and *Tg2*) varies between 0 (no glue) to 0.1, and 0.15 mm, as shown in Figure 15.

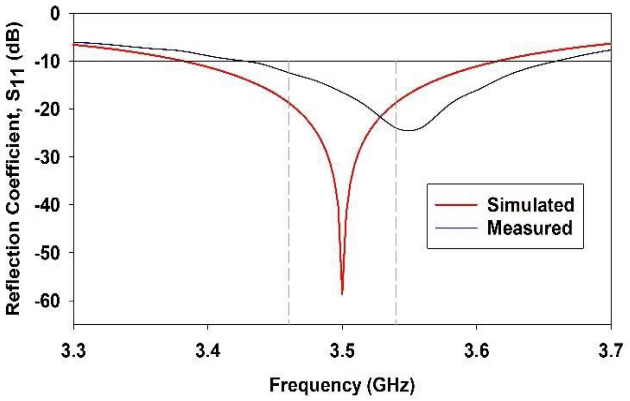

FIGURE 14. Simulated and measured reflection coefficient, S_{11} of antenna Step 4.

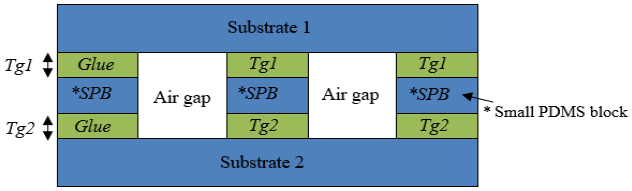

FIGURE 15. Illustration of antenna Step 4 with glue layers thickness of Tg1 and Tg2.

The reflection coefficient results of the re-simulated antenna in Step 4, with the varying existence of glue layers *Tg1* and *Tg2* are shown in Figure 16. It cleared the shifted frequency of the measured prototype antenna result was mainly due to the existence of thin glue layers between the substrates. The existence of glue on substrates 1 and 2 (Tg1 and Tg2 = 0.15 mm) was in good agreement with the measured prototype antenna.

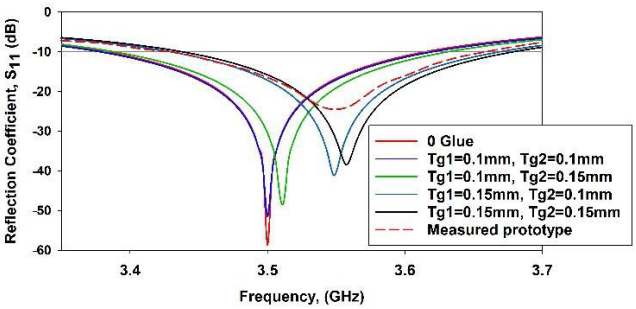

FIGURE 16. Simulated reflection coefficient of Antenna Step 4 when varying glue thickness *Tg1* and *Tg2*.

Meanwhile, the measured maximum gain and directivity of the prototype antenna (at 3.45 GHz) were 6.38 dBi and 7.69 dBi, respectively, which are in agreement with the simulated 6.23 dBi and 8.69 dBi, respectively. Figure 17 shows the simulated and measured normalised radiation patterns of the antenna in Step 4. The main lobe in the upper graph of the X-Z plane implies that the antenna radiation was dominant at the front of the antenna patch with minor lobe radiation at the back. The small lobe radiation at the back is a good deal for wearable antennas consider the specific absorption rate (SAR), radiation must be low for human safety.

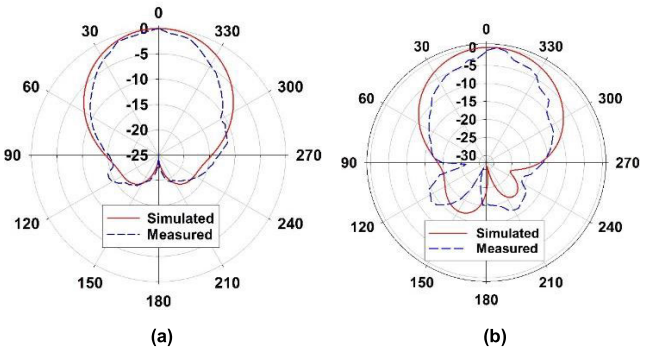

FIGURE 17. Simulated and measured radiation patterns of the antenna Step 4 (a) X-Z plane and (b) Y-Z plane.

B. STRETCH ANALYSIS

The stretch analysis for antenna Step 4 was conducted at the 10% and 20% stretch levels. A mechanical test was performed on the antenna prototype using a fixture, as shown in Figure 18 (a). The reflection coefficient of the stretch analysis for Antenna Step 4 is presented in Figure 18 (b). As expected, stretching the prototype antenna increased the patch length, resulting in a lower resonant frequency due to the nature of the microstrip patch antennas. This phenomenon is consistent with equation (6) [37], which relates the resonant frequency (f_r) of the antenna to the free space velocity (c), patch length (L), and effective dielectric constant (ε_{eff}). The empirical analytical equation used in previous studies [56], [57], [58] shows that the resonance frequency is inversely proportional to the electrical length along the direction of the current flow on the patch antenna. Therefore, an increase in the electrical size of the antenna stretching results in a longer wavelength and a lower resonant frequency.

$$f_r = \frac{c}{2L\sqrt{\varepsilon_{eff}}} \tag{6}$$

Figure 19 shows the directivity and gain measurements of the stretch antenna in step 4. The directivity and gain of the unstretched antenna are 7.96 dBi and 6.38 dBi, respectively. As the antenna is stretched to 10% and 20%, the directivity and gain values slightly decrease to 7.58 dBi and 5.75 dBi, respectively, and 7.42 dBi and 5.62 dBi, respectively. The reduction in antenna performance during stretching is primarily due to the piezoresistive effect. When mechanical strain is applied, the electrical resistivity of the material changes.

Consequently, the conductive pathways in the material are disrupted, causing separation of the conductive filler and decreased conductivity [37]. Disruption of the conductive path decreases the conductivity during stretching, as demonstrated in several studies [35], [59], [60]. This decrease in

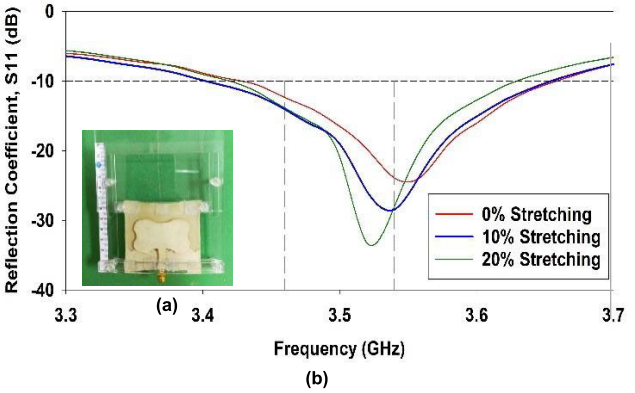

FIGURE 18. (a) Fixture to stretch the prototype antenna and (b) Measured reflection coefficient, S_{11} of antenna stretching.

conductivity negatively affects the gain and directivity performance of the antenna [27].

Figure 20 depicts the normalised radiation patterns of the prototype antenna under the influence of stretching. The radiation patterns of the stretched antenna exhibit a high degree of similarity to those of the unstretched antenna in terms of forward directivity radiation, with a minor lobe located at the back. Notably, the minor lobe of the stretched antenna exhibited a marginal reduction. Stretching of the antenna causes a considerable decrease in the back-lobe radiation, which leads to a reduction in antenna gain and a corresponding decrease in radiating power, resulting in a smaller amount of radiation at the back. Hence, this explains the significant drop in directivity and the significant reduction in back-lobe radiation when the antenna is stretched.

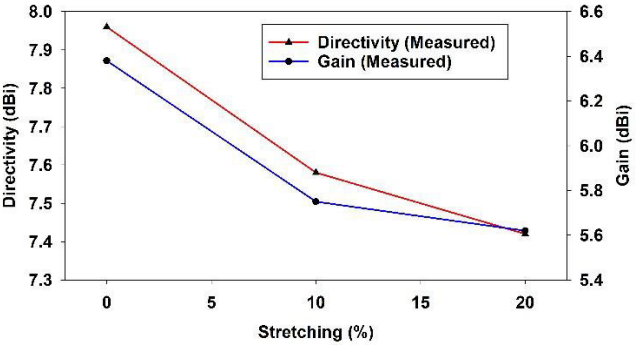

FIGURE 19. Measured of directivity and gain of prototype antenna during the stretching.

C. BENDING ANALYSIS

To emphasize the suitability of the prototype antenna for conformal wearable systems, it was tested at various bending angles. This was achieved by wrapping the wearable antenna around a plastic cylinder to model the bending that would occur when the antenna was deployed on a human arm, as depicted in Figure 21 (a). The antenna bending analysis covered angles of 21°, 30°, and 40°, taking into account

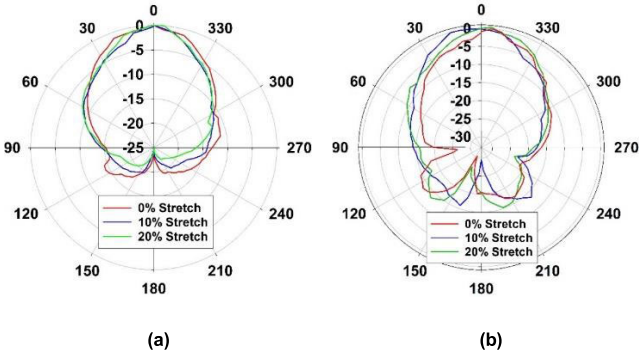

FIGURE 20. Measured radiation patterns of the prototype antenna stretching (a) X-Z plane and (b) Y-Z plane.

variations in human arm sizes for adults, teenagers, and children [61]. Each of these bending angles was analyzed four times, and the average value was considered as the result for each angle. The angles of the antenna bends reflected on the cylinder circumferences, which were selected based on being closed to midarm circumferences size group as tabulated in Table 1. The outer radius and circumference of the cylinder can be calculated using equations (7) and (8), respectively.

$$S = r\theta \tag{7}$$

$$C = 2r \tag{8}$$

The parameters for determining the antenna arc length involve S, the length of the arc, r, the radius of the circle, r, the central angle measured in radians, and C, the circumference of the cylinder or human arm. As the antenna was designed to bend along the X-axis, its width was considered for computing the arc length, as illustrated in Figure 21 (b).

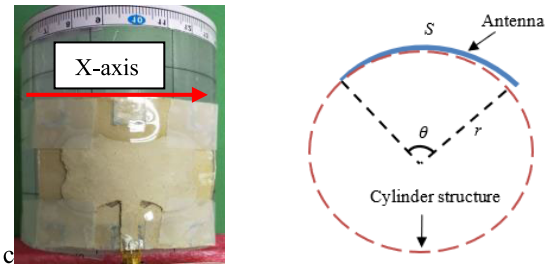

FIGURE 21. (a) Antenna prototype bent and (b) Cylindrical- rectangular patch cavity model for patch antenna bent on cylinder surface.

The measured reflection coefficient, S_{11}, of the antenna bent at different angles is shown in Figure 22. From the observation, the operating frequency of the bent antenna was shifted to a lower frequency as the antenna's bent angles increased. However, all shifted frequencies are in good agreement and operate in the 5G band as shown in Figure 22.

The impact of antenna bending on S_{11} can be understood through the application of the cylindrical-rectangular cavity theory. Elrashidi et al. [41], [62] presented the resonance

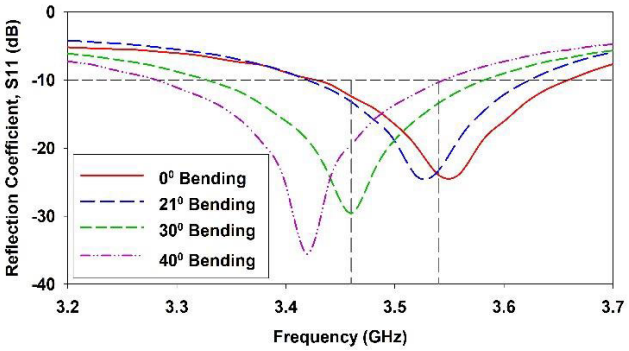

FIGURE 22. Measured reflection coefficient of antenna bending.

TABLE 1. The calculation of circumferences and angles of cylinder related to the midarm circumferences size [61].

Groups	Average midarm circumferences (cm)	Cylinder circumferences (cm)	Angles (degree)
Children	14.5 – 23.0	17.19	40
Teenagers	22.9 – 32.8	23.00	30
Adults	29.1 – 34.3	32.74	21

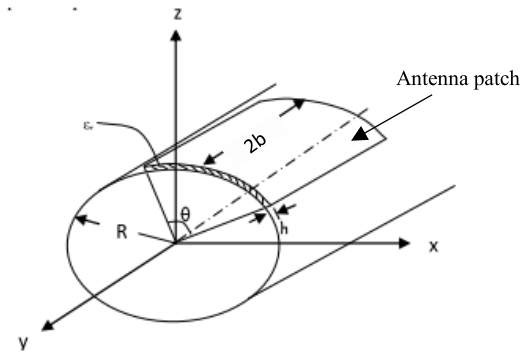

FIGURE 23. Cylindrical-rectangular cavity model for patch antenna bent on cylinder surface [63].

frequency modulation of conformal antennas caused by their curvature in this theory, which is denoted by:

$$(f_r)_{mn} = \frac{1}{2\sqrt{\mu\varepsilon}}\sqrt{\left(\frac{m}{2\theta a}\right)^2 + \left(\frac{n}{2b}\right)^2} \tag{9}$$

In Figure 23, the parameters for the patch antenna are defined as follows: μ represents the magnetic permeability, ε is the electric permittivity, 2θ is the angle that bounds the width of the patch, a is the radius of the cylinder, and 2b is the length of the patch antenna due to its bend in the H plane (longitudinal). The parameters m and n represent the number of mode orders for the transverse magnetic wave TMmn for H-plane bending and the transverse electric wave TEmn for E-plane bending [63]. Analytical equation (9) demonstrates that the angle θ of the antenna bending is not directly proportional to the resonance frequency. This explains why increasing the bending angle resulted in a decrease in the resonant frequency. Moreover, the curvature of the antenna creates an extended fringing field, that affects the resonance frequency, as referenced in [64]. The shift of the antenna bending towards a lower frequency is consistent with findings from other studies [26], [32], [66].

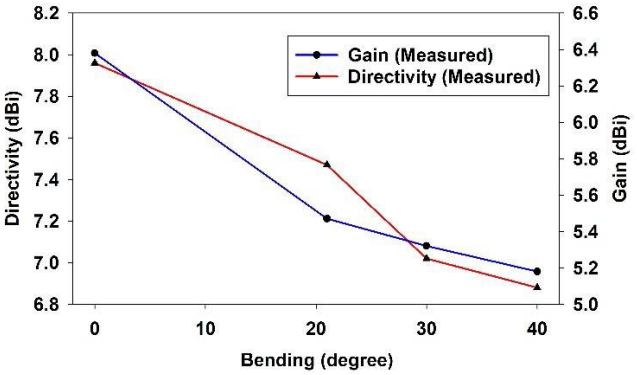

FIGURE 24. Measured directivity and gain of antenna bending.

The measured directivity and gain of the antenna bends are shown in Figure 24. The directivity of the antenna without a bend was 7.96 dBi and slightly decreased to 7.47 dBi, 7.02 dBi, and 6.88 dBi when the antenna was bent at 21°, 30°, and 40°, respectively. A similar decreasing pattern happens to the gain when antennas are bent (0° = 6.38 dBi, 21° = 5.47 dBi, 30° = 5.32 dBi, and 40° = 5.18 dBi). This result indicates that the decrease in directivity when the antenna is bent leads to a gain loss. The ground antenna was situated in the centre, sandwiched between a front patch and a back reflector. This arrangement resulted in the reflection of energy becoming confined within the bending region, as opposed to a flat antenna where the reflector plane can reflect the energy back to the front with greater efficiency. Additionally, the patch antenna is near the ground when it is bent, causing a fair amount of energy to couple into the ground, resulting in a decrease in energy propagation and gain loss [67].

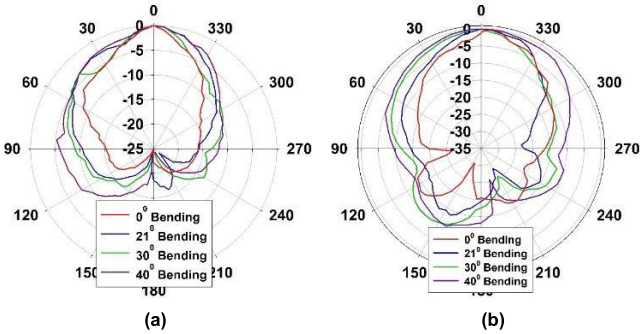

FIGURE 25. Measured radiation patterns of the prototype antenna bending (a) X-Z plane and (b) Y-Z plane.

The normalised radiation patterns of an antenna undergoing bending in both the X-Z and Y-Z planes are shown

TABLE 2. Previous reported polymer base wearable antennas comparison with proposed antenna.

Ref.	Substrate Materials	Conductive Materials	Conductivity (S/m)	Bandwidth (MHz)	Directivity	Gain (dBi)	Bending Analysis	Max. Stretch (%)
[71]	Polyester textile	Silver ink	N/A	110	N/A	3.6	Yes	N/A
[72]	NinjaFlex-thermoplastic polyurethane (TPU)	Silver conductive paste (DuPont PE872)	1.7×10^4	1120	4.67 dBi	-7.2	Yes	N/A
[73]	PDMS	AgNW/PDMS	8.13×10^5	239	4.16 dBi	0.37	Yes	15
[74]	Acrylic elastomer VHB Tape 4905	Ag(flakes), fluorine elastomer, organic solvent, surfactant.	8.49×10^4	Patch (500) Bow tie (2800)	N/A	N/A	No	Patch (65) Bow tie (110)
[37]	PDMS	Polysiloxane-silver ink composite	5.62×10^3	105	5.08 dBi	N/A	No	20
[75]	PDMS	Silver loaded epoxy	2.0×10^4	Antenna I (500) Antenna II (400)	Antenna I (58%) Antenna II (61%)	Antenna I (4.98) Antenna II (5.28)	No	N/A
This work	PDMS	Ag-PDMS composite paste	6.58×10^6	227	7.69 dBi	6.38	Yes	20

* N/A = Not available.

in Figure 25. The observed radiation patterns indicate that the bent antenna performs similarly to the unbent antenna, with the exception of a slightly larger back lobe resulting from the curvature of the antenna in the H-plane towards the rear. The primary front lobe of the antenna remains good under all bending conditions, indicating that most of the energy is propagated from the front patch of the antenna, which is beneficial for wearable antenna applications.

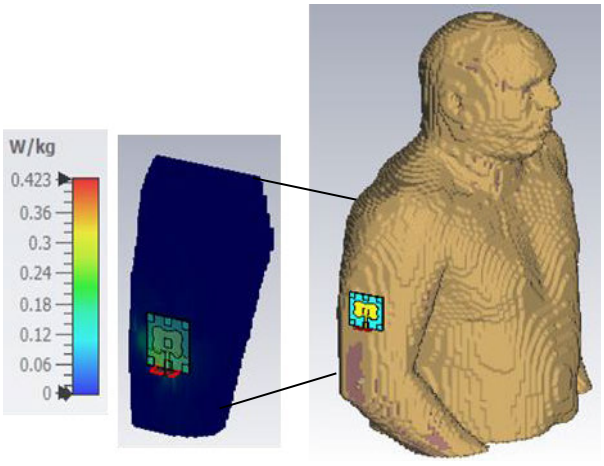

FIGURE 26. Simulated SAR value for 1g tissue.

D. SPECIFIC ABSORPTION RATE (SAR) ANALYSIS

As the wearable antenna was incorporated into the human body, its safety was investigated. To conduct this investigation, specific absorption rate (SAR) analysis was simulated using CST software. This analysis involved the utilization of Hugo human model tissue, with the antenna positioned on the centre arm, as shown in Figure 26. The SAR parameter is a defined measure for assessing the quantity of electromagnetic (EM) power generated by an antenna that is absorbed by human tissue, where SAR is expressed in units of watts per kilogram (W/kg) [67]. The Institute of Electrical and Electronics Engineers (IEEE) defines SAR as the time derivative of the incremental energy (dW) absorbed by dissipation in an incremental mass (dm) contained in a volume (dV) of a given density (ρ) [69], [70]. This can be expressed through the use of equation (10) [68], [70].

$$SAR = \frac{d}{dt}\left(\frac{dW}{dm}\right) = \frac{d}{dt}\left(\frac{dW}{\rho dV}\right) \tag{10}$$

In accordance with the relationship between absorbed power, sample volume, and mass density (where W represents absorbed power, V represents sample volume, and ρ represents mass density), numerical values were calculated for the maximum specific absorption rate (SAR) using the CST software. At 1g of tissue, the maximum SAR was determined to be 0.42 W/kg, while at 10g of tissue, the maximum SAR value was 0.19 W/kg. The slightly higher SAR value for 1g of tissue can be attributed to the fact that SAR absorption levels are dependent on the surface area. Specifically, the SAR for 10 g of tissue is distributed over a larger surface area, resulting in a lower density of radio frequency (RF) energy throughout the area. Both analyses revealed SAR values being well below

the maximum limits of 1.6 W/kg for 1g of tissue and 2 W/kg for 10g of tissue, which are established in IEEE standards for human exposure to radio frequency electromagnetic fields spanning the range of 3 KHz to 300 GHz (IEEE standard C95.1-1991) [68].

E. COMPARATIVE ANALYSIS OF PUBLISHED WORK PERFORMANCE AND PROPOSED ANTENNA

Table 2 provides a comparison between the proposed antenna and other wearable antennas in terms of conductivity, bandwidth, directivity, gain, and flexibility. The proposed antenna used an Ag-PDMS composite material with the highest conductivity value as well as could stretch and bend along the PDMS substrate material. This level of flexibility is not available for other wearable antennas that are limited to bending or stretching.

In addition, the proposed wearable antenna is the first to use an air gap between the substrates, which is achieved by integrating small PDMS blocks. This design, along with a sawtooth partial ground and reflector at the back, results in a gain of 6.38 dBi, which is the highest among the antennas compared. The proposed antenna was also tested for stretch, bending, and specific absorption rate (SAR) analysis and was found to be suitable for 5G wearable device applications. The size of the antenna (60 × 60 mm) is reasonable and can be easily attached to the human body. Overall, the proposed antenna has significant advantages over other wearable antennas in terms of conductivity, flexibility, and gain, making it a promising option for 5G devices.

IV. CONCLUSION

The focus of this study was to develop, design, analyse, and build a prototype of a wearable patch antenna for 5G electronic applications at 3.5 GHz, using a conductive silver paste based on a polymer composite as the antenna material. To achieve a flexible and compact wearable antenna, different silver weight percentage compositions of the silver conductive polymer composites were investigated. The use of a custom-made silver composite as a conductive antenna is promising for various research areas, not only wireless communication.

Initially, a conventional microstrip patch antenna was designed and analysed using the measured electrical properties of the conductive silver paste based on a polymer composite with a conductivity of 6.58×10^6 S/m. Subsequently, the antenna was enhanced by implementing small polydimethylsiloxane (PDMS) blocks between the substrates to create an air gap, adding a sawtooth partial ground, and adding a reflector at the back. This resulted in improved stretchability, bandwidth, and gain of up to 20%, 13.65%, and 6.38 dBi, respectively.

The proposed antenna was also subjected to mechanical stretch and bending analysis, which yielded results that were consistent with those of other studies. Moreover, the stretching and bending of the antenna maintained resonance in the 5G bandwidth with a high gain compared to previous wearable antennas. Finally, the preliminary specific absorption rate (SAR) of both antennas was analysed for safety purposes. The simulated SAR values for the antenna were within the safety limits for human exposure to electromagnetic frequencies.

The integration of an air gap substrate, partial ground, and reflector onto a microstrip patch antenna, as well as the use of silver paste based on polymer composites, has a significant impact on improving antenna performance, especially gain. The analyses of stretch, bending, and SAR also revealed competitive results for wearable antennas that can be integrated with upcoming 5G electronic devices. For future work, certain considerations must be taken into account, particularly when fabricating the antenna prototype. It is essential to measure the parameters of all the materials used in the antenna prototype before designing the antenna in simulation, as the choice of materials significantly affects the antenna's performance.

ACKNOWLEDGMENT

The authors would like to thank all the researchers with the School of Electrical and Electronic Engineering, School of Materials and Mineral Resources Engineering, Universiti Sains Malaysia, and the Advanced Communication Engineering (ACE), Center of Excellence, Faculty of Electronic Engineering and Technology, Universiti Malaysia Perlis.

REFERENCES

[1] T. S. Rappaport, S. Sun, R. Mayzus, H. Zhao, Y. Azar, K. Wang, G. N. Wong, J. K. Schulz, M. Samimi, and F. Gutierrez, "Millimeter wave mobile communications for 5G cellular: It will work!" *IEEE Access*, vol. 1, pp. 335–349, 2013, doi: 10.1109/ACCESS.2013.2260813.

[2] G. D. Kumar, "Design of 4×4 microstrip quasi-Yagi beam-steering antenna array operation at 3.5GHz for future 5G vehicle applications," *Int. J. Eng. Adv. Technol.*, vol. 7, no. 6, pp. 34–37, 2018.

[3] O. Vermesan and P. Friess, *Internet of Things: Converging Technologies for Smart Environments and Integrated Ecosystems* (River Publishers Series in Communications). Denmark, U.K.: River Publisher, Jan. 2013.

[4] K. N. Paracha, S. K. Abdul Rahim, P. J. Soh, and M. Khalily, "Wearable antennas: A review of materials, structures, and innovative features for autonomous communication and sensing," *IEEE Access*, vol. 7, pp. 56694–56712, 2019, doi: 10.1109/ACCESS.2019.2909146.

[5] T. Cisco, "CISCO: 2020 CISO benchmark report," *Comput. Fraud Secur.*, vol. 2020, no. 3, p. 4, 2020, doi: 10.1016/s1361-3723(20)30026-9.

[6] P. Raj and A. C. Raman, *The Internet of Things: Enabling Technologies, Platforms, and Use Cases*, vol. 5, no. 3. Boca Raton, FL, USA: CRC Press, 2017.

[7] Cisco Systems Inc. (2011). *CISCO Visual Networking Index: Global Mobile Data Traffic Forecast Update, 2015–2020*. Growth Lakel. [Online]. Available: http://www.cisco.com/en/U.S./solutions/collateral/ns341/ns525/ns537/ns705/ns827/white_paper_c11-520862.html

[8] M. Chan, D. Estève, J.-Y. Fourniols, C. Escriba, and E. Campo, "Smart wearable systems: Current status and future challenges," *Artif. Intell. Med.*, vol. 56, no. 3, pp. 137–156, Nov. 2012, doi: 10.1016/j.artmed.2012.09.003.

[9] P. Rennison and A. Andrews. (2014). *Technology Alone Will Not Drive the Success of Wearable Devices Says Beecham Research*. Realwire. [Online]. Available: https://www.realwire.com/releases/Technology-alone-will-not-drive-the-success-of-wearable-devices-says-Beecham

[10] S.-H. Li and J.-s. Li, "Smart patch wearable antenna on jeans textile for body wireless communication," in *Proc. 12th Int. Symp. Antennas, Propag. EM Theory (ISAPE)*, Dec. 2018, pp. 1–4, doi: 10.1109/ISAPE.2018.8634084.

[11] M. E. Lajevardi and M. Kamyab, "Ultraminiaturized metamaterial-inspired SIW textile antenna for off-body applications," *IEEE Antennas Wireless Propag. Lett.*, vol. 16, pp. 3155–3158, 2017, doi: 10.1109/LAWP.2017.2766201.

[12] X. Zhu, X. Liu, and H. Yang, "Compact dual-band wearable textile antenna based on quarter-mode substrate integrated waveguide," in *Proc. 9th Asia–Pacific Conf. Antennas Propag. (APCAP)*, Aug. 2020, pp. 1–2, doi: 10.1109/APCAP50217.2020.9246045.

[13] A. Kavitha and J. N. Swaminathan, "Design of flexible textile antenna using FR4, jeans cotton and Teflon substrates," *Microsyst. Technol.*, vol. 25, no. 4, pp. 1311–1320, Apr. 2019, doi: 10.1007/s00542-018-4068-y.

[14] S. G. Kirtania, A. W. Elger, M. R. Hasan, A. Wisniewska, K. Sekhar, T. Karacolak, and P. K. Sekhar, "Flexible antennas: A review," *Micromachines*, vol. 11, no. 9, p. 847, Sep. 2020, doi: 10.3390/mi11090847.

[15] A. S. M. Alqadami, B. Mohammed, K. S. Bialkowski, and A. Abbosh, "Fabrication and characterization of flexible polymer iron oxide composite substrate for the imaging antennas of wearable head imaging systems," *IEEE Antennas Wireless Propag. Lett.*, vol. 17, no. 8, pp. 1364–1368, Aug. 2018, doi: 10.1109/LAWP.2018.2841879.

[16] R. B. V. B. Simorangkir, Y. Yang, and K. P. Esselle, "Robust implementation of flexible wearable antennas with PDMS-embedded conductive fabric," in *Proc. 12th Eur. Conf. Antennas Propag. (EuCAP)*, Apr. 2018, pp. 1–5, doi: 10.1049/cp.2018.0846.

[17] A. S. M. Sayem, R. B. V. B. Simorangkir, K. P. Esselle, and R. M. Hashmi, "Feasibility study of PDMS embedded transparent conductive fabric for the realization of transparent flexible antennas," in *Proc. 13th Eur. Conf. Antennas Propag. (EuCAP)*, Mar. 2019, pp. 1–4.

[18] R. B. V. B. Simorangkir, Y. Yang, R. M. Hashmi, T. Björninen, K. P. Esselle, and L. Ukkonen, "Polydimethylsiloxane-embedded conductive fabric: Characterization and application for realization of robust passive and active flexible wearable antennas," *IEEE Access*, vol. 6, pp. 48102–48112, 2018, doi: 10.1109/ACCESS.2018.2867696.

[19] R. Joshi, C. Constantinides, S. K. Podilchak, M. N. Ramli, H. Lago, and P. J. Soh, "Robust and compact PDMS antennas for search and rescue operations and emergency communications," in *Proc. 12th Eur. Conf. Antennas Propag. (EuCAP)*, Apr. 2018, pp. 1–5, doi: 10.1049/cp.2018.0975.

[20] A. A. Bakar, F. Hasnan, A. R. Razali, A. F. A. Rahim, M. S. Osman, T. Ali, and R. Radzali, "Polydimethylsiloxane as a potential antenna substrate," *Acta Phys. Polonica A*, vol. 135, no. 5, pp. 938–941, May 2019, doi: 10.12693/aphyspola.135.938.

[21] R. A. Liyakath, A. Takshi, and G. Mumcu, "Multilayer stretchable conductors on polymer substrates for conformal and reconfigurable antennas," *IEEE Antennas Wireless Propag. Lett.*, vol. 12, pp. 603–606, 2013, doi: 10.1109/LAWP.2013.2260123.

[22] S. Hage-Ali, N. Tiercelin, P. Coquet, R. Sauleau, H. Fujita, V. Preobrazhensky, and P. Pernod, "A millimeter-wave microstrip antenna array on ultra-flexible micromachined polydimethylsiloxane (PDMS) polymer," *IEEE Antennas Wireless Propag. Lett.*, vol. 8, pp. 1306–1309, 2009, doi: 10.1109/LAWP.2009.2037590.

[23] R. Salvado, C. Loss, R. Gonçalves, and P. Pinho, "Textile materials for the design of wearable antennas: A survey," *Sensors*, vol. 12, no. 11, pp. 15841–15857, Nov. 2012, doi: 10.3390/s121115841.

[24] P. Salonen, M. Keskilammi, and Y. Rahmat-Samii, "Textile antennas: Effect of antenna bending on radiation pattern and efficiency," in *Proc. IEEE Antennas Propag. Soc. Int. Symp.*, Jul. 2008, pp. 4–7, doi: 10.1109/aps.2008.4619343.

[25] M. A. R. Osman, M. K. A. Rahim, N. A. Samsuri, M. K. Elbasheer, and M. E. Ali, "Textile UWB antenna bending and wet performances," *Int. J. Antennas Propag.*, vol. 2012, pp. 1–12, Mar. 2012, doi: 10.1155/2012/251682.

[26] A. Mersani, L. Osman, and J.-M. Ribero, "Effect of bending on the characteristics of a coplanar textile antenna," in *Proc. 18th Medit. Microw. Symp. (MMS)*, Oct. 2018, pp. 255–257, doi: 10.1109/MMS.2018.8612049.

[27] Q.-Y. Tang, Y.-M. Pan, Y. C. Chan, and K. W. Leung, "Frequency-tunable soft composite antennas for wireless sensing," *Sens. Actuators A, Phys.*, vol. 179, pp. 137–145, Jun. 2012, doi: 10.1016/j.sna.2012.03.024.

[28] C. Miozzi, F. Amato, and G. Marrocco, "Performance and durability of thread antennas as stretchable epidermal UHF RFID tags," *IEEE J. Radio Freq. Identificat.*, vol. 4, no. 4, pp. 398–405, Dec. 2020, doi: 10.1109/JRFID.2020.3001692.

[29] M. Oyharçabal, T. Olinga, M.-P. Foulc, S. Lacomme, E. Gontier, and V. Vigneras, "Influence of the morphology of polyaniline on the microwave absorption properties of epoxy polyaniline composites," *Compos. Sci. Technol.*, vol. 74, pp. 107–112, Jan. 2013, doi: 10.1016/j.compscitech.2012.10.016.

[30] T. Zhao, C. Hou, H. Zhang, R. Zhu, S. She, J. Wang, T. Li, Z. Liu, and B. Wei, "Electromagnetic wave absorbing properties of amorphous carbon nanotubes," *Sci. Rep.*, vol. 4, no. 1, pp. 1–7, Jul. 2014, doi: 10.1038/srep05619.

[31] H. A. Rahman and S. K. A. Rahim, "Dual band PDMS based flexible antenna for wearable application," in *IEEE MTT-S Int. Microw. Symp. Dig.*, Sep. 2015, pp. 193–194, doi: 10.1109/imws-bio.2015.7303843.

[32] R. B. V. B. Simorangkir, Y. Yang, L. Matekovits, and K. P. Esselle, "Dual-band dual-mode textile antenna on PDMS substrate for body-centric communications," *IEEE Antennas Wireless Propag. Lett.*, vol. 16, pp. 677–680, 2017, doi: 10.1109/LAWP.2016.2598729.

[33] J. Trajkovikj, J.-F. Zürcher, and A. K. Skrivervik, "PDMS, a robust casing for flexible W-BAN antennas [EurAAP Corner]," *IEEE Antennas Propag. Mag.*, vol. 55, no. 5, pp. 287–297, Oct. 2013, doi: 10.1109/MAP.2013.6735538.

[34] S. Morris, A. R. Chandran, N. Timmons, and J. Morrison, "Design and performance of a flexible and conformal PDMS Dipole antenna for WBAN applications," in *Proc. 46th Eur. Microw. Conf. (EuMC)*, Oct. 2016, pp. 84–87, doi: 10.1109/EuMC.2016.7824283.

[35] B. S. Kim, K.-Y. Shin, J. B. Pyo, J. Lee, J. G. Son, S.-S. Lee, and J. H. Park, "Reversibly stretchable, optically transparent radio-frequency antennas based on wavy Ag nanowire networks," *ACS Appl. Mater. Interface*, vol. 8, no. 4, pp. 2582–2590, Feb. 2016, doi: 10.1021/acsami.5b10317.

[36] C. A. Balanis, *Antenna Theory: Analysis and Design*. Hoboken, NJ, USA: Wiley, 2010.

[37] M. R. Ramli, S. Ibrahim, Z. Ahmad, I. S. Z. Abidin, and M. F. Ain, "Stretchable conductive ink based on polysiloxane–silver composite and its application as a frequency reconfigurable patch antenna for wearable electronics," *ACS Appl. Mater. Interface*, vol. 11, no. 31, pp. 28033–28042, Aug. 2019, doi: 10.1021/acsami.9b07671.

[38] W. L. Tham, W. S. Chow, and Z. A. M. Ishak, "The effect of 3-(trimethoxysilyl) propyl methacrylate on the mechanical, thermal, and morphological properties of poly(methyl methacrylate)/hydroxyapatite composites," *J. Appl. Polym. Sci.*, vol. 118, no. 1, pp. 218–228, Oct. 2010, doi: 10.1002/app.32111.

[39] J. C. J. Bart, *Additives in Polymers: Industrial Analysis and Applications*, 2005.

[40] D. M. Pozar, "Microstrip antennas," *Proc. IEEE*, vol. 80, no. 1, pp. 79–91, Jan. 1992, doi: 10.1109/5.119568.

[41] A. Elrashidi, K. Elleithy, and H. Bajwa, "Performance analysis of a microstrip printed antenna conformed on cylindrical body at resonance frequency 4.6 GHz for TM01 mode," *Proc. Comput. Sci.*, vol. 10, pp. 775–784, Jan. 2012, doi: 10.1016/j.procs.2012.06.099.

[42] N. Rajasekhar, R. R. Reddy, and N. K. Darimireddy, "V-shaped slits and a slot loaded pentagonal boundary patch antennas for wideband applications," in *Proc. IEEE Int. Conf. Antenna Innov. Modern Technol. Ground, Aircr. Satell. Appl. (iAIM)*, Nov. 2017, pp. 1–5, doi: 10.1109/IAIM.2017.8402600.

[43] R. K. Garg, S. Dwivedi, and R. Tomar, "A wide band, highly-efficient circular patch antenna with split triangular-shape slit," in *Proc. 8th Int. Conf. Commun. Syst. Netw. Technol. (CSNT)*, Nov. 2018, pp. 1–5, doi: 10.1109/CSNT.2018.8820273.

[44] K. S. Rao, D. R. Jahagirdar, and D. Ramakrishna, "Compact broadband asymmetric slit circularly polarized microstrip patch antenna for GPS and GLONASS applications," in *Proc. IEEE Int. Conf. Antenna Innov. Modern Technol. Ground, Aircr. Satell. Appl. (iAIM)*, Nov. 2017, pp. 1–3, doi: 10.1109/IAIM.2017.8402558.

[45] S. Arulmurugan, T. R. Sureshkumar, and Z. C. Alex, "Compact wearable microstrip patch antenna for 2.4 GHz using loaded slits and shorting pins," in *Proc. Emerg. Trends Ind. 4.0 (ETI)*, May 2021, pp. 1–5, doi: 10.1109/ETI4.051663.2021.9619435.

[46] A. Elakas, G. A. Imrak, M. Sencan, and S. T. Imeci, "Microstrip patch antenna with triangular slits," in *Proc. Int. Appl. Comput. Electromagn. Soc. Symp. (ACES)*, Mar. 2018, pp. 1–2, doi: 10.23919/ROPACES.2018.8364311.

[47] A. Kumar, N. Gupta, and P. C. Gautam, "Gain and bandwidth enhancement techniques in microstrip patch antennas—A review," *Int. J. Comput. Appl.*, vol. 148, no. 7, pp. 9–14, Aug. 2016, doi: 10.5120/ijca2016911207.

[48] R. Cicchetti, E. Miozzi, and O. Testa, "Wideband and UWB antennas for wireless applications: A comprehensive review," *Int. J. Antennas Propag.*, vol. 2017, pp. 1–45, Feb. 2017.
[49] M. T. Islam, R. Azim, and A. T. Mobashsher, "Triple band-notched planar UWB antenna using parasitic strips," *Prog. Electromagn. Res.*, vol. 129, pp. 161–179, 2012, doi: 10.2528/pier12032604.
[50] K. Jassim and R. H. Thaher, "Design and analysis microstrip antenna with reflector to enhancement gain for wireless communication," *Bull. Electr. Eng. Informat.*, vol. 9, no. 2, pp. 652–660, Apr. 2020, doi: 10.11591/eei.v9i2.1696.
[51] O. Ismail, L. Youssef, O. Otman, and A. Aghanim, "Design of a circular patch antenna with a reflector for GPR applications," in *Proc. ITM Web Conf.*, vol. 48, 2022, Art. no. 01004.
[52] C.-E. Guan and T. Fujimoto, "Reflector-backed microstrip patch antenna for medical body area network," in *Proc. 8th Asia–Pacific Conf. Antennas Propag. (APCAP)*, Aug. 2019, pp. 144–145, doi: 10.1109/APCAP47827.2019.9472025.
[53] G. Brist, S. Hall, S. Clouser, and T. Liang, "Non-classical conductor losses due to copper foil roughness and treatment," in *Proc. IPC Electron. Circuits World Conv.*, vol. 2, 2005, pp. 898–908.
[54] Y. Shlepnev and C. Nwachukwu, "Practical methodology for analyzing the effect of conductor roughness on signal losses and dispersion in interconnects," in *Proc. DesignCon*, vol. 4, 2012, pp. 2931–2955.
[55] S. Baua, G. Gampala, and C. J. Reddy, "Effect of surface roughness on antenna array for automotive radar applications," in *Proc. Int. Appl. Comput. Electromagn. Soc. Symp. (ACES)*, Aug. 2021, pp. 1–3.
[56] J. Zhu, J. J. Fox, N. Yi, and H. Cheng, "Structural design for stretchable microstrip antennas," *ACS Appl. Mater. Interface*, vol. 11, no. 9, pp. 8867–8877, Mar. 2019, doi: 10.1021/acsami.8b22021.
[57] S. Cheng and Z. Wu, "A microfluidic, reversibly stretchable, large-area wireless strain sensor," *Adv. Funct. Mater.*, vol. 21, no. 12, pp. 2282–2290, Jun. 2011, doi: 10.1002/adfm.201002508.
[58] Z. Wu, K. Hjort, and S. H. Jeong, "Microfluidic stretchable radio-frequency devices," *Proc. IEEE*, vol. 103, no. 7, pp. 1211–1225, Jul. 2015, doi: 10.1109/JPROC.2015.2395716.
[59] Z. Chen, J. Xi, W. Huang, and M. M. F. Yuen, "Stretchable conductive elastomer for wireless wearable communication applications," *Sci. Rep.*, vol. 7, no. 1, pp. 1–8, Sep. 2017, doi: 10.1038/s41598-017-11392-w.
[60] C. Feng and L.Y. Jiang, "Investigation of uniaxial stretching effects on the electrical conductivity of CNT–polymer nanocomposites," *J. Phys. D, Appl. Phys.*, vol. 47, no. 40, Oct. 2014, Art. no. 405103, doi: 10.1088/0022-3727/47/40/405103.
[61] C. D. Fryar, Q. Gu, C. L. Ogden, and K. M. Flegal, *Anthropometric Reference Data for Children Adults: United States*, no. 39. Hyattsville, MD, USA: DHHS Publication, 2016, pp. 2011–2014.
[62] K. Luk, K. Lee, and J. Dahele, "On the cylindrical-rectangular microstrip antenna," in *Proc. Antennas Propag. Soc. Int. Symp.*, Jun. 1987, pp. 1028–1031, doi: 10.1109/aps.1987.1149971.
[63] L. Song and Y. Rahmat-Samii, "A systematic investigation of rectangular patch antenna bending effects for wearable applications," *IEEE Trans. Antennas Propag.*, vol. 66, no. 5, pp. 2219–2228, May 2018, doi: 10.1109/TAP.2018.2809469.
[64] A. Elrashidi, K. Elleithy, and H. Bajwa, "The fringing field and resonance frequency of cylindrical microstrip printed antenna as a function of curvature," *Int. J. Wireless Commun. Netw.*, vol. 7, pp. 583–600, Jun. 2001. [Online]. Available: https://citeseerx.ist.psu.edu/viewdoc/citations;jsessionid=74F31254B4B73E7EDABDB01DE50F4828?doi=10.1.1.678.8736
[65] M. Haerinia and S. Noghanian, "Study of bending effects on a dual-band implantable antenna," in *Proc. IEEE Int. Symp. Antennas Propag. USNC-URSI Radio Sci. Meeting*, Jul. 2019, pp. 753–754, doi: 10.1109/APUSNCURSINRSM.2019.8888320.
[66] H.-L. Kao, C.-L. Cho, X.Y. Zhang, L.-C. Chang, B.-H. Wei, X. Dai, and H.-C. Chiu, "Bending effect of an inkjet-printed series-fed two-dipole antenna on a liquid crystal polymer substrate," *IEEE Antennas Wireless Propag. Lett.*, vol. 13, pp. 1172–1175, 2014, doi: 10.1109/LAWP.2014.2330819.
[67] H. Yalduz, T. E. Tabaru, V.T. Kilic, and M. Turkmen, "Design and analysis of low profile and low SAR full-textile UWB wearable antenna with metamaterial for WBAN applications," *AEU Int. J. Electron. Commun.*, vol. 126, Nov. 2020, Art. no. 153465, doi: 10.1016/j.aeue.2020.153465.
[68] *IEEE Standard for Safety Levels With Respect to Human Exposure to Radio Frequency Electromagnetic Fields, 3 kHz to 300 GHz*, Standard C95.1-2005, Institute of Electrical and Electronics Engineers, 1999.
[69] A. Nazeri, A. Abdolali, and M. Mehdi, "An extremely safe low-SAR antenna with study of its electromagnetic biological effects on human head," *Wireless Pers. Commun.*, vol. 109, no. 2, pp. 1449–1462, Nov. 2019, doi: 10.1007/s11277-019-06621-6.
[70] A. Shah and P. Patel, "Suspended embroidered triangular e-textile broadband antenna loaded with shorting pins," *AEU Int. J. Electron. Commun.*, vol. 130, Feb. 2021, Art. no. 153573, doi: 10.1016/j.aeue.2020.153573.
[71] S. B. Roshni, M. P. Jayakrishnan, P. Mohanan, and K. P. Surendran, "Design and fabrication of an E-shaped wearable textile antenna on PVB-coated hydrophobic polyester fabric," *Smart Mater. Struct.*, vol. 26, no. 10, Oct. 2017, Art. no. 105011, doi: 10.1088/1361-665x/aa7c40.
[72] M. Rizwan, M. W. A. Khan, L. Sydänheimo, J. Virkki, and L. Ukkonen, "Flexible and stretchable brush-painted wearable antenna on a three-dimensional (3-D) printed substrate," *IEEE Antennas Wireless Propag. Lett.*, vol. 16, pp. 3108–3112, 2017, doi: 10.1109/LAWP.2017.2763743.
[73] L. Song, A. C. Myers, J. J. Adams, and Y. Zhu, "Stretchable and reversibly deformable radio frequency antennas based on silver nanowires," *ACS Appl. Mater. Interface*, vol. 6, no. 6, pp. 4248–4253, Mar. 2014, doi: 10.1021/am405972e.
[74] H. Saghlatoon, M. M. Honari, R. Mirzavand, P. Mousavi, A. Kumar, T. G. La, and H.-J. Chung, "A novel investigation on printed stretchable WLAN antennas," in *Proc. IEEE Int. Symp. Antennas Propag. USNC/URSI Nat. Radio Sci. Meeting*, Jul. 2017, pp. 2537–2538, doi: 10.1109/APUSNCURSINRSM.2017.8073311.
[75] H. A. Rahman, S. K. A. Rahim, M. Abedian, and N. Najib, "Design of a flexible antenna using printed silver loaded epoxy on PDMS/plastic substrate for wearable applications," in *Proc. 10th Eur. Conf. Antennas Propag. (EuCAP)*, Apr. 2016, pp. 1–4, doi: 10.1109/EuCAP.2016.7481327.

SHAKHIRUL MAT SALLEH received the bachelor's and master's degrees in communication engineering from Universiti Malaysia Perlis (UniMAP), in 2013 and 2016, respectively. He is currently pursuing the Ph.D. degree in electrical and electronic engineering with Universiti Sains Malaysia (USM). In addition, he is a Lecturer with the Faculty of Electronic Engineering and Technology, Universiti Malaysia Perlis. His current research interests include wireless communication systems, antenna design, textile antennas, wearable antennas, flexible material antennas, reconfigurable antennas, and AMC antennas.

MOHD FADZIL AIN received the B.S. degree in electronic engineering from Universiti Teknologi Malaysia, Malaysia, in 1997, the M.S. degree in radio frequency and microwave from Universiti Sains Malaysia (USM), Malaysia, in 1999, and the Ph.D. degree in radio frequency and microwave from the University of Birmingham, U.K., in 2003. In 2003, he joined the School of Electrical and Electronic Engineering, USM. He is currently a Professor with VK7 Grade, the Dean of Research, Postgraduate, and Networking, and the Director of the Collaborative Microelectronic Design Excellence Centre (CEDEC). He is actively involved in technical consultancy with several companies in repairing microwave equipment. His current research interests include MIMO wireless systems on FPGA/DSP, Ka-band transceiver design, dielectric antenna, RF characterization of dielectric material, and microwave propagation study. His awards and honors include the International Invention Innovation Industrial Design and Technology Exhibition, the International Exposition of Research and Inventions of Institutions of Higher Learning, the Malaysia Technology Expo, the Malaysian Association of Research Scientists, the Seoul International Invention Fair, IENA, the Best Paper for the Seventh WSEAS International Conference on Data Networks, Communications, Computers, and the International Conference on X-Ray and Related Techniques in Research and Industry.

ZULKIFLI AHMAD received the Ph.D. degree in polymer chemistry from the University of Reading, U.K. He is currently a Professor with the School of Material and Mineral Resources Engineering, Universiti Sains Malaysia, Engineering Campus. He is a Malaysian National Expert in polymer synthesis and polymer electronics. He has supervised eight Ph.D. and eight M.Sc. students. He has secured several research grants, including the Bridging Fund from USM for the fabrication of stretchable organic transistor, RUI for the study on stress and reliability of advanced interconnection materials for flexible hybrid electronics applications, and FRGS for the design of crosslink networks for improvement of thermal conductivity in interface material. He has been a member of the Royal Chemical Society, since 2014.

INTAN SORFINA ZAINAL ABIDIN (Member, IEEE) received the M.Eng. degree in electronics engineering from the University of Surrey, Guildford, U.K., in 2008, and the Ph.D. degree from the 5G Innovation Centre (5GIC), Institute of Communication System (ICS), University of Surrey, in 2017. Then, she was with Motorola Solutions (M), Penang, Malaysia, as an Electrical Engineer, for two years, before moving to Celestica (M), Kulim, Malaysia, to work as a Product Engineer. She is currently a Senior Lecturer with the School of Electrical and Electronic Engineering, Universiti Sains Malaysia (USM), specializing in electronics communication systems, antenna, channel propagation, RF, microwave engineering, and MIMO systems.

LEE YENG SENG (Senior Member, IEEE) received the bachelor's (Hons.) and Ph.D. degrees in communication engineering, in 2012 and 2016, respectively. From 2012 to 2018, he published 31 journals, 23 conference papers, four book chapters, and three books. His current research interests include microwave engineering, dielectric material characterization, microwave absorbers, electromagnetic, antenna design, and frequency selective surface (FSS). He is a member of IET, MBOT, and BEM.

MOHAMED NASRUN OSMAN was born in Jitra, Malaysia, in 1987. He received the Electrical Engineering degree in telecommunication and the Ph.D. degree in electrical engineering from Universiti Teknologi Malaysia, in 2010 and 2016, respectively. He is currently a Senior Lecturer with Universiti Malaysia Perlis, Malaysia. His current research interests include reconfigurable antenna design, RF design, and wireless multi-in multi-out systems.